



HAL
open science

Steady solutions in Lattice-Boltzmann computations of turbulent flows: a method based on selective frequency damping

Jérôme Jacob, Christophe Friess

► **To cite this version:**

Jérôme Jacob, Christophe Friess. Steady solutions in Lattice-Boltzmann computations of turbulent flows: a method based on selective frequency damping. 25e Congrès Français de Mécanique, Aug 2022, Nantes, France. hal-04280178

HAL Id: hal-04280178

<https://hal.science/hal-04280178v1>

Submitted on 10 Nov 2023

HAL is a multi-disciplinary open access archive for the deposit and dissemination of scientific research documents, whether they are published or not. The documents may come from teaching and research institutions in France or abroad, or from public or private research centers.

L'archive ouverte pluridisciplinaire **HAL**, est destinée au dépôt et à la diffusion de documents scientifiques de niveau recherche, publiés ou non, émanant des établissements d'enseignement et de recherche français ou étrangers, des laboratoires publics ou privés.

Steady solutions in Lattice-Boltzmann computations of turbulent flows: a method based on selective frequency damping

J. Jacob^a, C. Friess^b

a. M2P2 UMR 7340, Aix-Marseille Université, CNRS, Centrale Marseille, jerome.jacob@univ-amu.fr

b. M2P2 UMR 7340, Aix-Marseille Université, CNRS, Centrale Marseille,
christophe.friess@univ-amu.fr

Résumé :

The present study deals with the issue of convergence in Lattice-Boltzmann computations of turbulent flows using the Reynolds-Averaged Navier-Stokes (RANS) approach. A method to improve the convergence is proposed. It is inspired from the work of [1], regarding selective frequency damping (SFD). Preliminary results of the method are shown. The studied case is the flow around a cylinder at Reynolds number $Re = 140000$.

Mots-clefs : Lattice-Boltzmann method, RANS, selective frequency damping

1 Introduction

The lattice-Boltzmann method (LBM) is a kinetic approach for computational fluid dynamics. In LBM, flow variables, e.g. density, velocity, are directly obtained from microscopic particle properties. The advantages of the LBM are its parallelism, simple structure, simplicity in coding, and the straightforward incorporation of microscopic interactions. However, when applied to steady flows, the standard LBM usually converges rather slowly, and the time-consuming convergence progress prevents it from being as competitive as conventional CFD methods in practical applications.

Rather sophisticated approaches to circumvent this problem, have been proposed, e.g. [2] using a preconditioning of the solver. In the present study, we take an alternative path, by investigating the capability of the selective frequency damping (SFD) method, initially introduced by [1] to improve the convergence of an LBM solution towards its steady state. The challenge lies in the fact that the SFD method was initially developed in the framework of Navier-Stokes solvers.

2 Numerical model

The fluid dynamics equations are solved using the Lattice Boltzmann Method ([3]) which describes the evolution of the density distribution of particles ($f_\alpha(\mathbf{x}, t)$) with velocity \mathbf{c}_α on a $DnQm$ lattice (n dimensions and m velocities). The hybrid recursive regularized lattice Boltzmann model presented in [4] is used in the present work leading to the following lattice Boltzmann equation:

$$f_\alpha(\mathbf{x} + \mathbf{c}_\alpha \delta_t, t + \delta_t) = f_\alpha^{eq}(\mathbf{x}, t) + \left(1 - \frac{1}{\tau}\right) f_\alpha^{neq}(\mathbf{x}, t) + \frac{1}{2} \mathbf{F}_\alpha(\mathbf{x}, t) \quad (1)$$

where f_α^{eq} is the equilibrium distribution function, f_α^{neq} the off equilibrium distribution function and \mathbf{F}_α an external force discretized on the *DnQm* lattice following [5] method. The relaxation time τ is given from the molecular (ν) and turbulent (ν_t) viscosity following:

$$\tau = \frac{1}{2} + \frac{\nu + \nu_t}{c_s^2} \quad (2)$$

where c_s^2 represents the speed of sound. The turbulent viscosity is obtained here using the f_{v3} formulation of the Spalart-Allmaras model (*SA - f_{v3}* , [6]) as described in [7].

3 Forcing method

The forcing method consists of an additional bulk force \mathbf{F} . It is based on the selective frequency damping (SFD) introduced by [1] with the purpose of selectively damping frequencies in the momentum signal. Its expression, in the i -th spatial direction is:

$$F_i = -\chi (u_i - \bar{u}_i) , \quad (3)$$

where \bar{u} is the averaged velocity and χ is a factor with the dimension of a frequency. Following Cahuzac et al.[8], the average velocity is dynamically estimated using exponentially weighted moving average:

$$\bar{u}_i(t + \delta t) = (1 - c_{exp})\bar{u}_i(t) + c_{exp}u_i(t + \delta t) , \quad (4)$$

with:

$$c_{exp} = 3.628f_c\delta t , \quad (5)$$

where f_c is the cutoff frequency of the selected filter, and δt the time step.

One can see that the challenge of the SFD method is twofold: (i) using a proper dynamical estimate of the averaged velocity during the computation and (ii) calibrating the frequency χ to reach the best compromise between convergence speed of the solution and its accuracy. More recently, the SFD method has been improved (see e.g. [9]) based on mathematical considerations.

4 Results

The SFD method, used in the Lattice-Boltzmann framework, is tested for the flow around a cylinder with a Reynolds number of 140000. The computation domain is extended 10 and 30 diameters in the upstream and downstream directions and 15 diameters in the crosswind directions leading to a blockage ratio of 3.22%. The grid is composed of several embedded subdomains with uniform grid with a ratio of 2 in the grid spacing between two successive subdomains. In the present case the minimal grid size is $D/80$ (with D the cylinder diameter) around the cylinder and $D/10$ far from the cylinder. In all the presented simulations, the SFD method is arbitrarily activated after $50D/U_0$ and the simulation are performed for $200D/U_0$.

In order to assess the efficiency of the method, the streamwise velocity at 3 different locations in the wake (see Fig 1) and the cylinder drag force are extracted along time.

The values of the parameters χ and f_c are expressed in terms of the vortex-shedding frequency f_s , which is $f_s \approx 4200\text{Hz}$ in the present test case considering a Strouhal number $St \approx 0.2$ at $\text{Re} = 140000$ [10].

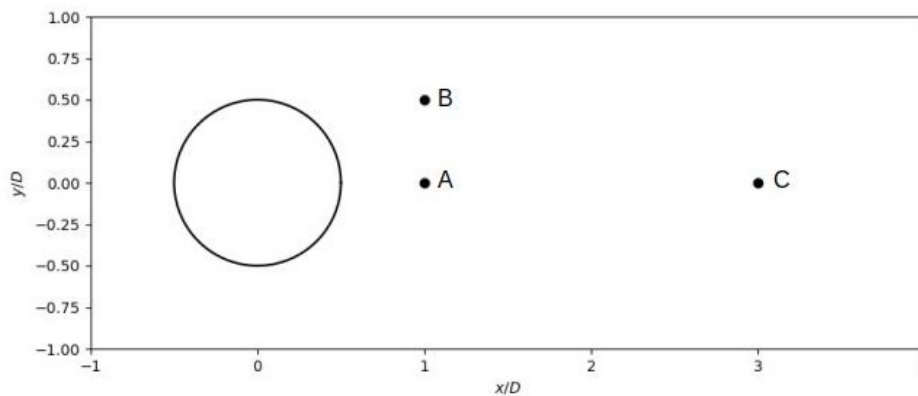


Figure 1: Location of the wake velocity sensors.

χ	$0 f_s$	$5 f_s$	$20 f_s$	$50 f_s$	$100 f_s$	$200 f_s$	$500 f_s$
L_r/D	0.8	1.12	0.9	0.85	0.83	0.82	0.81
U_{min}/U_0	-0.268	-0.349	-0.309	-0.288	-0.279	-0.274	-0.270

Table 1: Evolution of the recirculation length (L_r) and minimal velocity in the wake centerline (U_{min}) with χ values for the imposed averaged velocity configuration.

4.1 Target averaged velocity taken from a previous computation

First, in order to determine relevant values of χ , we compute the SFD method with a fixed target average, taken from post-processing a previous computation, performed without SFD.

Figure 2 shows an instantaneous map of the streamwise velocity field, around and downstream the cylinder, for various values of the frequency χ : 0 (without forcing), 5, 50 and 500 f_s . The first observation is that for all non-zero values of χ , the velocity map is pretty symmetric with respect to the plane $y = 0$, which features a steady-state solution, while the non-forced case is clearly unsteady. Besides, the case with $\chi = 5 f_s$ exhibits a longer recirculation bubble than the other cases.

This is confirmed by Table 1, which indicates the length of the recirculation bubble and the minimal velocity in the wake centerline, for several values of χ , compared with the non-forced case ($\chi = 0 f_s$). Interestingly, the prediction of this quantities improves when χ increases.

Figure 3 shows the time evolution of the streamwise velocity, taken at points A, B and C. The target velocity is displayed for comparison. Interestingly, the higher values of χ imply not only a faster convergence of the velocity, but also the converged state is reasonably close to the reference time-average, at all three considered points. At the opposite, low values of χ lead to a significant velocity discrepancy, as well as a slightly slower convergence.

Figure 4 compares the time evolution of the drag coefficient C_x obtained with the various values of χ used above. It is worth noticing that at $t = 50D/U_0$, when the forcing starts, the drag coefficient adapts abruptly, and converges rapidly toward a steady state. One can observe that, unlike the velocities:

- C_x converges faster toward its steady state at intermediate values of χ .
- The discrepancy in C_x (when compared with its reference value) is non monotonous in χ : the lowest χ does not yield the worst value C_x .

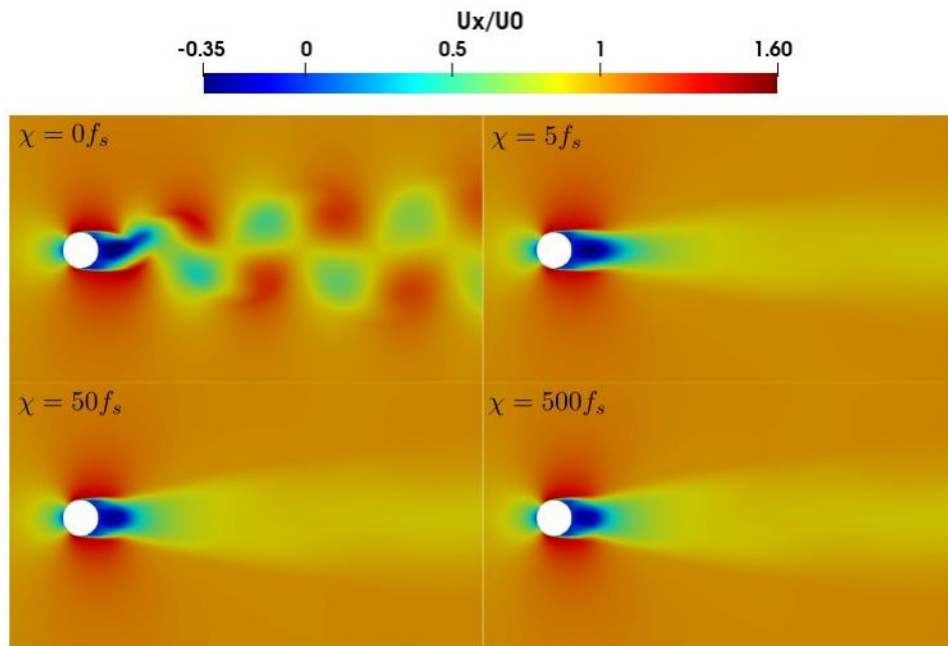


Figure 2: Visualisation of the normalized streamwise velocity field around the cylinder for different χ values and imposed averaged velocity after $200D/U_0$.

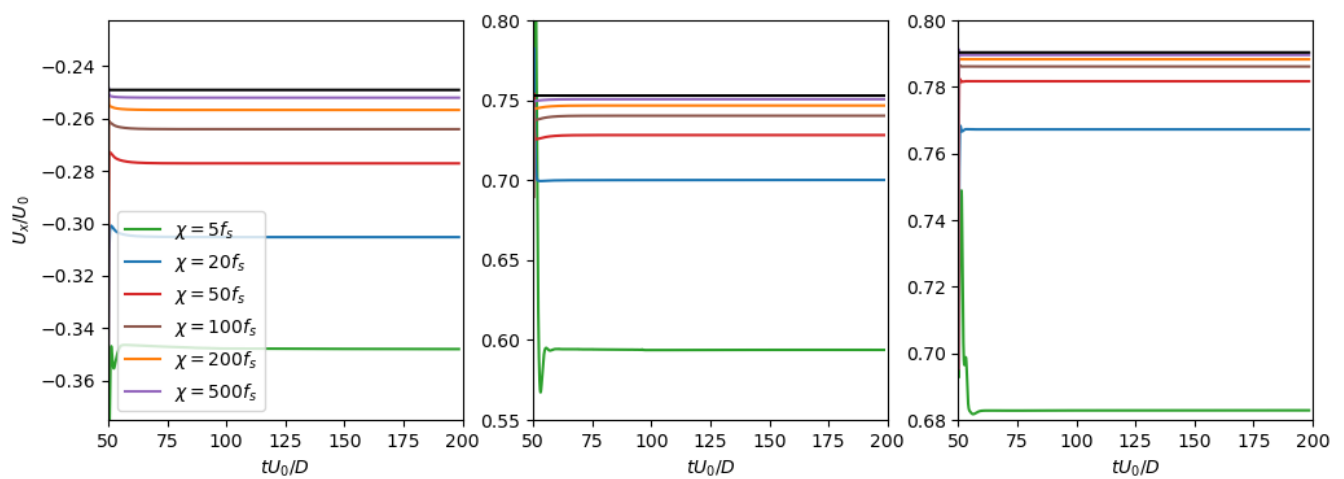


Figure 3: Time evolution of the streamwise velocity at point A, B and C (from left to right) for different χ values and imposed average velocity field. The target velocity is marked with the black line.

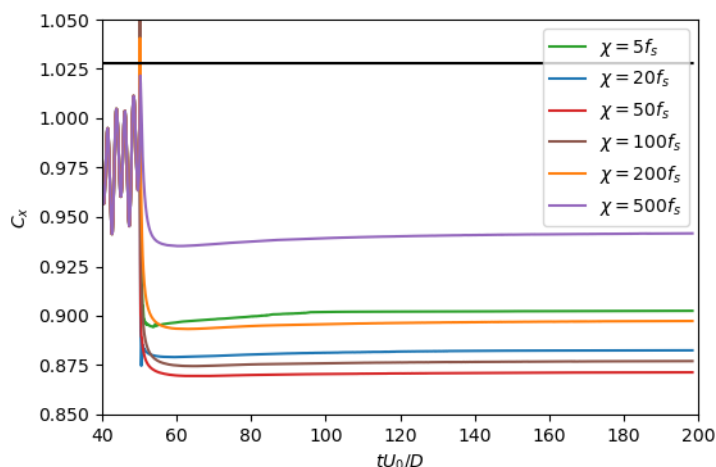


Figure 4: Time evolution of the drag coefficient for different χ values and imposed average velocity field. The target drag coefficient is marked with the black line.

However, the highest value of χ exhibits the best converged value of the drag coefficient (with a discrepancy around 7.3%).

4.2 Dynamic average

The main goal of the presented method, is to achieve steady RANS solutions in Lattice-Boltzmann computations, particularly in order to save computational resources. Indeed, without a specific treatment, it is necessary to run a sufficiently long computation to ensure the convergence of the time-averaged quantities of the flow. To this aim, the present section focuses on how to compute a dynamic time-average during the computation, and whether this time-average is accurate and efficient.

Figure 5 shows the time evolution of the streamwise velocity, taken at points A, B and C, for various values of f_c , χ being fixed at $500 f_s$, which is the most efficient value in the static-average case, discussed in Section 4.1. The target velocity is displayed for comparison. Interestingly, the velocity signals do not perfectly converge asymptotically: they exhibit a drift which is smaller when f_c is small, and vice-versa. This is due to the fact that a small f_c slowly affects the dynamic average (see Eqs. 4 and 5).

The point A is within the recirculation bubble: the streamwise velocity is negative. All values of f_c fulfill this criterion, except for $f_c = f_s/32$. This might be due to a bad convergence of the averaged velocity, especially since the velocity signal exhibits an oscillatory phase before its convergence (observed at points B and C as well). A similar oscillatory phase is observed for $f_c = f_s/16$, but not at higher values of f_c .

The choice $f_c = f_s/8$ constitutes some compromise between fastness of convergence (no oscillatory phase when the forcing is switched on) and robustness of the obtained averaged velocity, i.e. a smaller drift. However, it leads to discrepant values of the velocity.

Figure 6 shows the time evolution of the streamwise velocity at points A, B and C for different values of χ , when keeping $f_c = f_s/8$. As observed when using a static average velocity, taken from a previous computation (see Sec. 4.1), the value $\chi = 500 f_s$ leads to the best results: not only it exhibits the fastest convergence (however with a small drift), but also the velocity discrepancy with respect to its target value, is the smallest.

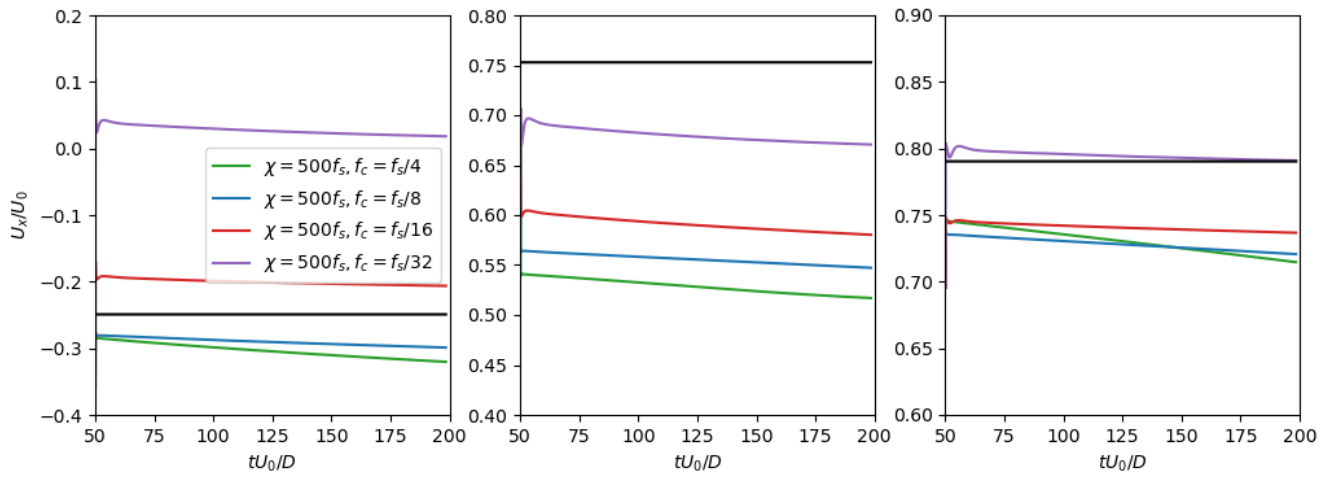


Figure 5: Time evolution of the streamwise velocity at point A, B and C (from left to right) for different f_c values with $\chi = 500f_s$. The target velocity is marked with the black line.

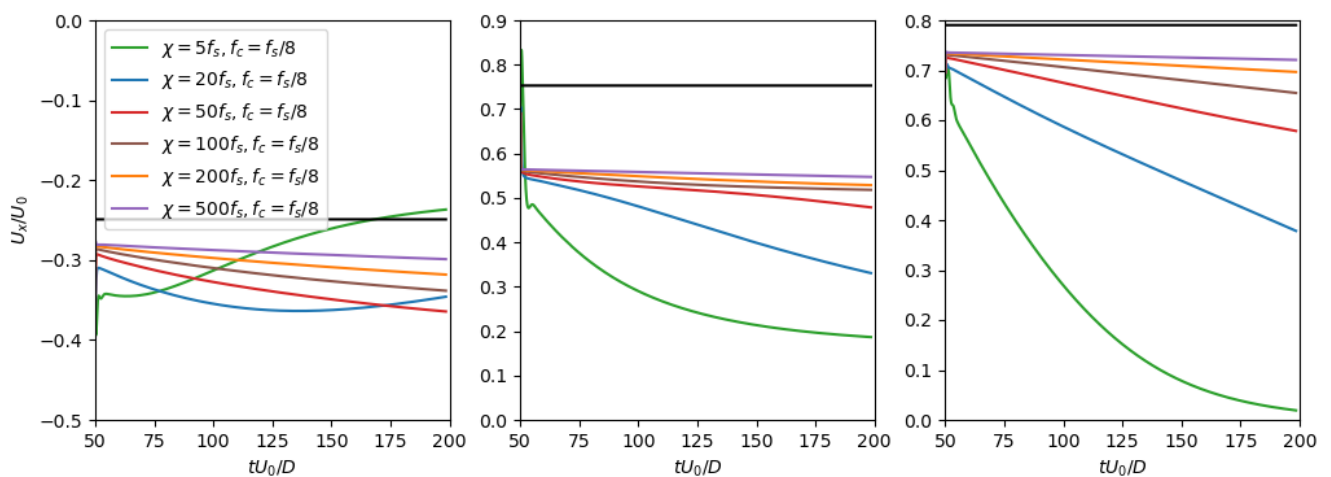


Figure 6: Time evolution of the streamwise velocity at point A, B and C (from left to right) for different χ values with $f_c = f_s/8$. The target velocity is marked with the black line.

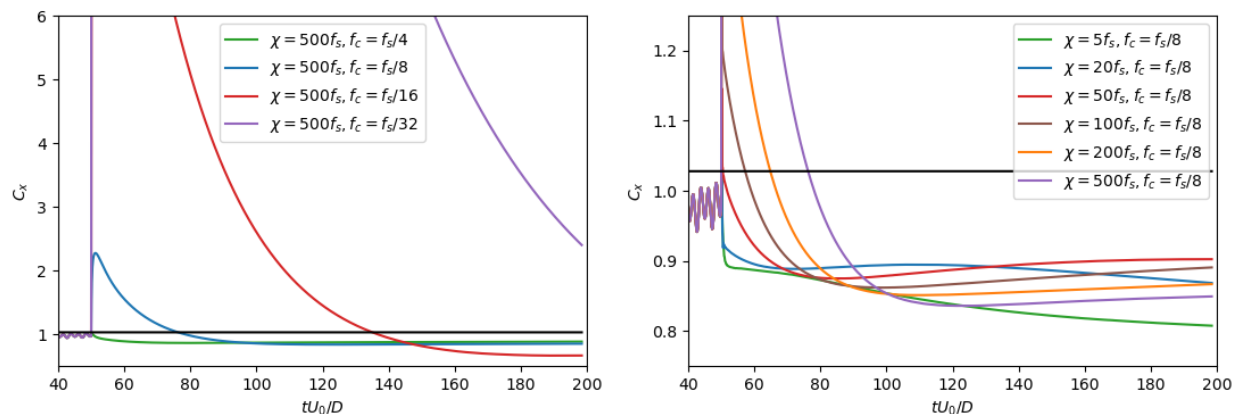


Figure 7: Time evolution of the drag coefficient for different f_c with $\chi = 500f_s$ (left) and different χ values with $f_c = f_s/8$ (right). The target drag coefficient is marked with the black line.

Figure 7 compares the time evolution of the drag coefficient C_x obtained with

- the various values of f_c used above, with fixed $\chi = 500f_s$.
- various values of χ used previously, with fixed $f_c = f_s/8$.

It is worth noticing that, just like the static case (see Fig. 4), when the forcing starts, the drag coefficient adapts abruptly, and converges rapidly toward a steady state. One can also note that this abrupt jump at $t = 50D/U_0$ is far weaker for $f_c = f_s/4$ and $f_c = f_s/8$ and seem to converge toward an acceptable value for C_x . Moreover, the converged values of C_x for $f_c = f_s/4$ and $f_c = f_s/8$ are the closest to the reference.

Now, when keeping $f_c = f_s/8$ constant and varying χ , all asymptotic values of C_x seem to be between 10% and 20% underestimated, when comparing with the reference drag coefficient. However, the higher χ is, the better the solution seems to convergence toward a constant C_x , in terms of both fastness and accuracy. Nevertheless, small drifts are observed at all values of χ . These observations are slightly different from those made in the static case (see Section 4.1).

4.3 Reynolds number effect

The study has been extended to other Reynolds numbers, namely $Re = 3900$ and 400000 . Time evolution of the streamwise velocity at points A, B and C are shown on Fig. 8, while the time evolution of the drag coefficient is shown on Fig. 9. The proportional gain of the forcing, χ is set too $500f_s$ and the cutoff frequency f_c is set to $f_s/8$. In both cases the vortex shedding frequency f_s was estimated considering the Strouhal number $St \approx 0.21$ for $Re = 3900$ [11] and $St \approx 0.46$ for $Re = 400000$ [12].

Qualitatively, the same observations as for $Re = 140000$, can be made at $Re = 3900$ and 400000 . Regarding the streamwise velocity, the prediction is reasonably accurate, at all three points. However, the velocity signal undergoes a small drift, especially at point A, which is within the close wake centerline.

Regarding the drag coefficient, it is slightly underestimated, in comparison with the reference C_x , similarly as for $Re = 140000$. Interestingly, the abrupt jump observed immediately after the forcing is switched on, already observed at $Re = 140000$ (see Figs. 4 and 7), appears at $Re = 3900$, but not at $Re = 400000$.

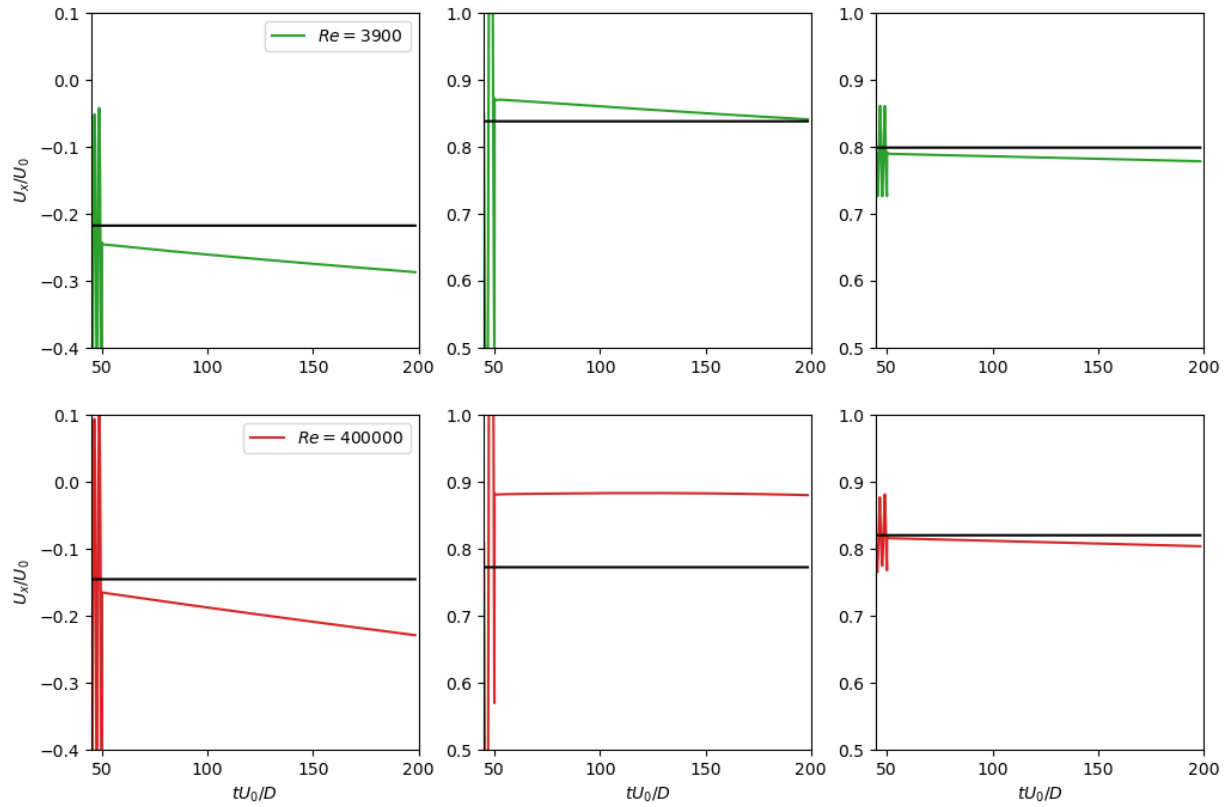


Figure 8: Time evolution of the streamwise velocity at point A, B and C (from left to right) for different Reynolds number with $\chi = 500f_s$ and $f_c = f_s/8$. The target velocity is marked with the black line.

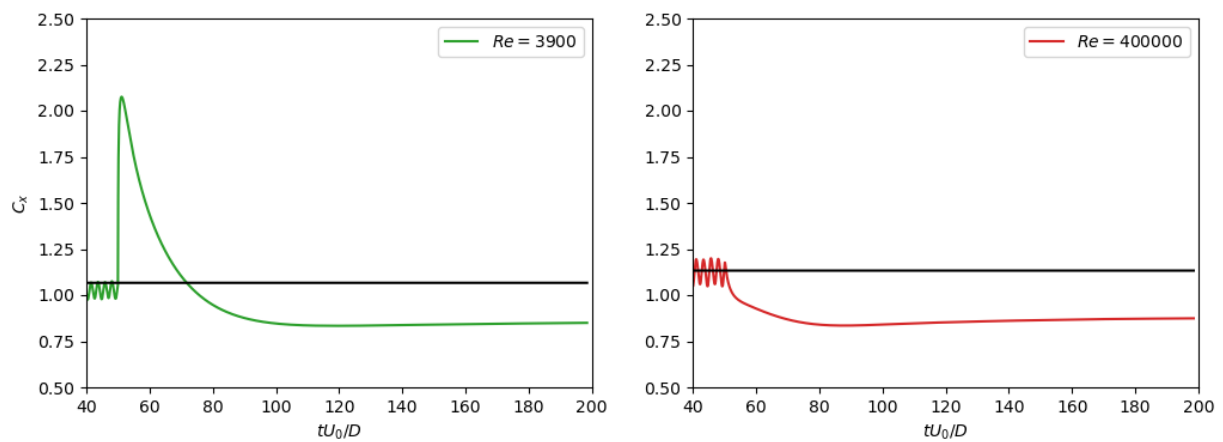


Figure 9: Time evolution of the drag coefficient for different Reynolds number with $\chi = 500f_s$ and $f_c = f_s/8$. The target drag coefficient is marked with the black line.

5 Conclusion

A method to improve convergence in Lattice-Boltzmann RANS computations, has been presented. This method is based on selective frequency damping, and consists in adding, in the LBM equations, a volume force driving velocity toward its average. This force acts like an active control device, and its key parameter is a proportional gain, here called χ . Preliminary tests of this method, have been performed in the case of the flow around a cylinder, at various Reynolds numbers.

At $Re = 140000$, it has been shown that, when using a static target average, taken from post-processing a previous calculation, high values of the proportional gain χ allow an overall better convergence of the solution, except for the drag coefficient on the cylinder.

Using a dynamic average for the forcing, raises the issue of computing the temporal average of the velocity. In the present study, an exponentially weighted moving average, is used. This moving average is based on a cutoff frequency f_c , whose choice is non-trivial: if f_c is too low, the computed time average may not respond fast enough to significant changes in the flow. On the contrary, if f_c is too high, the time average may respond too fast. The results of this preliminary study, confirm this non-triviality: the velocity hardly converges toward a constant value, and undergoes a small drift, for any value of f_c . Another key issue is when to start forcing the flow. Since using a static average leads to consistent results, one can safely assume that the dynamic time average of the flow just needs to be properly calculated, so that the forcing does not drive the flow toward an undesired state. On the other hand, a motivation of the present method is also to reduce computational cost. Therefore, an initial average-computing phase, without forcing, must be short enough to meet the aforementioned criterion.

Similar observations were made at $Re = 3900$ and $Re = 400000$. $Re = 20000$ has been tested as well, but not shown here. It appears that the velocity average was poorly converged, thus forcing the flow toward an undesired steady state, significantly discrepant from the reference state.

Besides, oddly enough, regardless of the averaging strategy (static or dynamic), and regardless of the forcing parameters χ and f_c , and for any of the studied Reynolds numbers, the resulting drag coefficient of the cylinder is always lower than its reference value.

The most crucial future improvement of the method, lies in the computation of a proper dynamic time-average of the velocity. Kalman filtering will be considered in future work. Moreover, one can put interest in the energy balance, which is modified by the proposed forcing. Indeed, from a URANS point of view, the SFD forcing removes turbulent kinetic energy from the resolved large scales. This should be compensated in the turbulence model, which accounts for the unresolved scales. The theoretical derivation of this term, in the framework of the Spalart-Allmaras model, though far from easy, will be the next step of this study.

References

- [1] E. Åkervik, L. Brandt, D. S. Henningson, J. Hoepffner, O. Marxen, and P. Schlatter, “Steady solutions of the Navier-Stokes equations by selective frequency damping,” *Physics of fluids*, vol. 18, no. 6, p. 068102, 2006.
- [2] A. De Rosis, “Preconditioned lattice boltzmann method for steady flows: A noncascaded central-moments-based approach,” *Physical Review E*, vol. 96, no. 6, p. 063308, 2017.

- [3] T. Krüger, H. Kusumaatmaja, A. Kuzmin, O. Shardt, G. Silva, and E. M. Vigen, “The lattice Boltzmann method,” *Springer International Publishing*, vol. 10, no. 978-3, pp. 4–15, 2017.
- [4] J. Jacob, O. Malaspinas, and P. Sagaut, “A new hybrid recursive regularised Bhatnagar–Gross–Krook collision model for lattice Boltzmann method-based large eddy simulation,” *Journal of Turbulence*, vol. 19, no. 11-12, pp. 1051–1076, 2018.
- [5] Z. Guo, C. Zheng, and B. Shi, “Discrete lattice effects on the forcing term in the lattice Boltzmann method,” *Physical review E*, vol. 65, no. 4, p. 046308, 2002.
- [6] S. R. Allmaras and F. T. Johnson, “Modifications and clarifications for the implementation of the spalart-allmaras turbulence model,” in *Seventh international conference on computational fluid dynamics (ICCFD7)*, vol. 1902, Big Island, HI, 2012.
- [7] S. Wilhelm, J. Jacob, and P. Sagaut, “An explicit power-law-based wall model for lattice Boltzmann method–Reynolds-averaged numerical simulations of the flow around airfoils,” *Physics of Fluids*, vol. 30, no. 6, p. 065111, 2018.
- [8] A. Cahuzac, J. Boudet, P. Borgnat, and E. Lévêque, “Smoothing algorithms for mean-flow extraction in large-eddy simulation of complex turbulent flows,” *Physics of fluids*, vol. 22, no. 12, p. 125104, 2010.
- [9] B. E. Jordi, C. J. Cotter, and S. J. Sherwin, “An adaptive selective frequency damping method,” *Physics of Fluids*, vol. 27, no. 9, p. 094104, 2015.
- [10] M. Breuer, “A challenging test case for large eddy simulation: high reynolds number circular cylinder flow,” *International journal of heat and fluid flow*, vol. 21, no. 5, pp. 648–654, 2000.
- [11] P. Parnaudeau, J. Carlier, D. Heitz, and E. Lamballais, “Experimental and numerical studies of the flow over a circular cylinder at reynolds number 3900,” *Physics of Fluids*, vol. 20, no. 8, p. 085101, 2008.
- [12] P. W. Bearman, “On vortex shedding from a circular cylinder in the critical reynolds number regime,” *Journal of Fluid Mechanics*, vol. 37, no. 3, pp. 577–585, 1969.